Article

Simulation of *S*-Entropy Production during the Transport of Non-Electrolyte Solutions in the Double-Membrane System

Andrzej Ślęzak [1], Wioletta M. Bajdur [1,*], Kornelia M. Batko [2,*] and Radomir Ščurek [3]

[1] Department of Innovation and Safety Management Systems, Technical University of Czestochowa, 42200 Czestochowa, Poland; aslezak52@gmail.com
[2] Department of Business Informatics, University of Economics, 40287 Katowice, Poland
[3] Department of Security Services, Faculty of Safety Engineering, VSB-Ostrava, 70030 Ostrava, Czech Republic; radomir.scurek@vsb.cz
* Correspondence: wiolawb@poczta.onet.pl (W.M.B.); kornelia.batko@ue.katowice.pl (K.M.B.)

check for
updates

Abstract: Using the classical Kedem–Katchalsky' membrane transport theory, a mathematical model was developed and the original concentration volume flux (J_v), solute flux (J_s) characteristics, and *S*-entropy production by J_v, $\left((\psi_S)_{J_v}\right)$ and by J_s $\left((\psi_S)_{J_s}\right)$ in a double-membrane system were simulated. In this system, M_1 and M_r membranes separated the *l*, *m*, and *r* compartments containing homogeneous solutions of one non-electrolytic substance. The compartment *m* consists of the infinitesimal layer of solution and its volume fulfills the condition $V_m \rightarrow 0$. The volume of compartments *l* and *r* fulfills the condition $V_l = V_r \rightarrow \infty$. At the initial moment, the concentrations of the solution in the cell satisfy the condition $C_l < C_m < C_r$. Based on this model, for fixed values of transport parameters of membranes (i.e., the reflection (σ_l, σ_r), hydraulic permeability (L_{pl}, L_{pr}), and solute permeability (ω_l, ω_r) coefficients), the original dependencies $C_m = f(C_l - C_r)$, $J_v = f(C_l - C_r)$, $J_s = f(C_l - C_r)$, $(\Psi_S)_{J_v} = f(C_l - C_r)$, $(\Psi_S)_{J_s} = f(C_l - C_r)$, $R_v = f(C_l - C_r)$, and $R_s = f(C_l - C_r)$ were calculated. Each of the obtained features was specially arranged as a pair of parabola, hyperbola, or other complex curves.

Keywords: membrane transport; Kedem–Katchalsky equations; double-membrane system; nonlinear model equations; *S*-entropy production

1. Introduction

One of the most important properties of each non-equilibrium thermodynamic system is the continuous production of *S*-entropy [1,2]. The temporal change in *S*-entropy is a consequence of the entropy exchange with the external environment (φ_S) and the entropy production in the system (ψ_S). This means that for irreversible processes occurring in open systems, the *S*-entropy rate of change (dS/dt) is the sum of the rate of entropy exchange with the external environment ($\varphi_S = d_eS/dt < 0$ or $d_eS/dt > 0$) and the rate of entropy production in the system as a result of irreversible processes ($\psi_S = d_iS/dt > 0$) [1–3]. The rate of entropy production can be expressed using the expression $\Psi_S = \sum_i J_i X_i$, where $J_i X_i$ is the product of the conjugate forces (X_i) and fluxes (J_i). Prigogine [4] showed that for systems far from equilibrium, in the area of applicability of the extended non-equilibrium thermodynamics (ENET), $d\psi_s/dt = d_J\psi_S/dt + d_X\psi_S/dt =$ where $d_J\psi_S/dt \equiv \sum_i J_i(dX_i/dt)$, $d_X\psi_S/dt \equiv \sum_i X_i(dJ_i/dt)$, and $d_X\psi_S/dt \leq 0$. Furthermore, $d_J\psi_S/dt \leq 0$, in the regime of applicability of linear non-equilibrium thermodynamics (LNET).

Membrane transport processes on the nano-, micro-, and macro-scale are the subject of interest in different areas of human activity in science, technology, and medicine [5–9]. One of the most

important scientific achievements in this area is the double-membrane model proposed by Curran and McIntosh. This model requires the existence of two membranes (M_l, M_r) with various hydraulic permeability (L_{pl}, L_{pr}), reflection (σ_l, σ_r), and solute permeability (ω_l, ω_r) coefficients, arranged in series and separating the solutions with different concentrations (C_l, C_m, C_r) [10]. Papers published over several years have been dedicated to the analysis of transport in the double-membrane cell in order to clarify certain biophysical aspects of the membrane transport of water and dissolved substances, both in biological and artificial systems [11–19]. Recently, a double-membrane transducer protector [8] and double-membrane triple-electrolyte redox flow battery design [9] have been developed based on the concept of the two-membrane system.

On the basis of the characteristics illustrating the impact of concentration, pressure, and voltage dependencies on the volume flow, solute flow, and electric current, it has been shown that transport, in compliance with the concentration gradient, iso-osmotic transport, and the passive transport (against the concentration gradient), is possible in this system [11,12]. In addition, it has been shown that the double-membrane system is characterized by rectifying and amplification properties (asymmetry current-voltage characteristics [13–19]) and asymmetry and amplification of the volume and solute fluxes and hydromechanics pressure, which is characteristic for biological systems [20–23].

In the present paper, with the use of the Curran–Kedem–Katchalsky method utilized in the following papers [10–17,20–23], a non-linear mathematical model of transport in the double-membrane osmotic-diffusive cell was developed. This cell contains two membranes (M_l, M_r) arranged in series and separating the compartments (l), (m), and (r), which contain the solutions of various concentrations, respectively, C_l, C_m, and C_r (at the initial moment $C_l > C_m > C_r$ or $C_l < C_m < C_r$). The volume of these compartments satisfies the conditions: $V_m \rightarrow 0$ and $V_l = V_r \rightarrow \infty$. Transport properties of the membranes M_l and M_r are characterized by coefficients of hydraulic permeability (L_{pl}, L_{pr}), reflection (σ_l, σ_r), and solute permeability (ω_l, ω_r). In order to search for new transport properties of the double-membrane system on the basis of the mathematical model, the calculations of the concentration (C_m), volume flux (J_v), solute flux (J_s), S-entropy produced by J_v, $\left((\psi_S)_{J_v}\right)$ and by J_s $((\psi_S)_{J_s})$, and osmotic and diffusion resistances (R_v, R_s).

2. Theory

2.1. Membrane System

Like in [7,8], let us consider the membrane system represented schematically in Figure 1. In this system, the compartments (l), (m), and (r), containing binary solutions of the same substance with the concentrations C_l, C_m, and C_r ($C_l > C_m > C_r$) are separated by electroneutral and selective membranes (M_l, M_r). The hydrostatic pressures in these compartments are denoted by P_l, P_m, and P_r ($P_l > P_m > P_r$) The membranes are characterized by the hydraulic permeability (L_{pl}, L_{pr}), reflections (σ_l, σ_r), and solute permeability (ω_l, ω_r). Compartment (m) consists of the infinitesimal layer of solution with the concentration C_m. The volume of this compartment fulfills the condition $V_m \rightarrow 0$. The volumes of the compartments (l) and (r), containing solutions with the concentration C_l and C_r, fulfill the condition $V_l = V_r \rightarrow \infty$.

The analysis of transport processes in this membrane system was based on the classical Kedem–Katchalsky model equations [15] using the Curran–Kedem–Katchalsky method [10,14,15]. Our starting point was the classical Kedem–Katchalsky model equations in binary and non-ionic solutions

$$J_s = \omega\Delta\pi + J_v(1-\sigma)\overline{C} \tag{1}$$

$$J_v = L_p(\Delta P - \sigma\Delta\pi) \tag{2}$$

where J_s and J_v are the solute and volume fluxes; ω is the solute permeability coefficient; σ is the reflection coefficient; L_p is the hydraulic permeability coefficient; $\Delta\pi = RT\Delta C$ is the osmotic pressure difference (RT is the product of the gas constant and absolute temperature); $\overline{C}$ is the average solution

concentration in the membrane; and ΔP is the hydrostatic pressure difference. Equation (1) describes the solute flux, the first component of this equation, $J_{sd} = \omega\Delta\pi$, describes the diffusive flux, and the second, $J_{sa} = J_v(1 - \sigma)\,\overline{C}$, is the advective flux. Then, Equation (2) describes the volume flux. It serves to note that the first component of this equation, $J_{vh} = L_p\Delta P$, is the hydraulic volume flux, and the second one, $J_{vo} = L_p\sigma\Delta\pi$, is the osmotic volume flux.
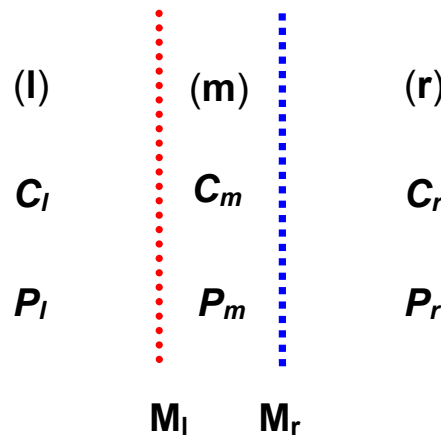
Figure 1. Model of double-membrane system: M_l, M_r = membranes; l, m, r = compartments; P_h, P_m, P_l = mechanical pressures; C_l, C_m, C_r = concentrations of solutions.

2.2. Model Equations

In order to describe the stationary volume flux in the membrane system shown in Figure 1, we considered Equation (1). The equations for membranes M_l and M_r are written in the following forms:

$$J_{sl} = \omega_l RT(C_l - C_m) + J_{vl}(1 - \sigma_l)\overline{C}_l \tag{3}$$

$$J_{sr} = \omega_r RT(C_m - C_r) + J_{vr}(1 - \sigma_r)\overline{C}_r \tag{4}$$

where $\overline{C}_l = (C_l - C_m)[\ln(C_l C_m{}^{-1})]^{-1} \approx \frac{1}{2}(C_l + C_m)$, and $\overline{C}_r = (C_m - C_r)[\ln(C_m C_r{}^{-1})]^{-1} \approx \frac{1}{2}(C_m + C_r)$.

In the steady state, the following conditions are fulfilled:

$$J_{sl} = J_{sh} = J_s \tag{5}$$

$$J_{vl} = J_{vr} = J_v \tag{6}$$

On the basis of Equations (3)–(6), we obtain

$$C_m = \frac{RT(\omega_l C_l + \omega_r C_r) + \frac{1}{2}J_v[(1 - \sigma_l)C_l - (1 - \sigma_r)C_r]}{RT(\omega_l + \omega_r) + \frac{1}{2}J_v(\sigma_l - \sigma_r)} \tag{7}$$

In order to calculate J_v, on the basis of Equation (2) for the membrane system presented in Figure 1, we can write

$$J_{vl} = L_{pl}(P_l - P_m) - L_{pl}\sigma_l RT(C_l - C_m) \tag{8}$$

$$J_{vr} = L_{pr}(P_m - P_r) - L_{pr}\sigma_r RT(C_m - C_r) \tag{9}$$

Combining Equations (6), (8), and (9), we obtain the equation describing hydrostatic pressure in the intermembrane compartment of the double-membrane system

$$P_m = \frac{L_{pl}P_l + L_{pr}P_r - RT\left(L_{pl}\sigma_l C_l + L_{pr}\sigma_r C_r\right) + C_m RT\left(L_{pl}\sigma_l + L_{pr}\sigma_r\right)}{L_{pl} + L_{pr}} \tag{10}$$

Taking into consideration Equations (8) and (10), we obtain

$$J_v = \frac{L_{pl}L_{pr}}{L_{pl} + L_{pr}}[(P_l - P_r) + RT(\sigma_r C_r - \sigma_l C_l) + RTC_m(\sigma_l - \sigma_r)] \tag{11}$$

Including Equation (11) into Equation (7), we derive

$$\alpha_1 C_m{}^2 + \alpha_2 C_m + \alpha_3 = 0 \tag{12}$$

where $\alpha_1 = L_{pl}L_{pr}RT(\sigma_l - \sigma_r)^2$; $\alpha_2 = 2RT(L_{pl} + L_{pr})(\omega_l + \omega_r) + L_{pl}L_{pr}(\sigma_l - \sigma_r)[(P_l - P_r) - RT(C_l - C_r)]$; and $\alpha_3 = -2RT(L_{pl} + L_{pr})(\omega_l C_l + \omega_r C_r) - L_{pl}L_{pr}[(1 - \sigma_l)C_l - (1 - \sigma_r)C_r][(P_l - P_r) + RT(\sigma_r C_r - \sigma_l C_l)]$.

Hereby, we obtain the equation describing the solution concentration in the intermembrane compartment of the double-membrane system. Taking into consideration Equations (7) and (11), we obtain

$$\beta_1 J_v{}^2 + \beta_2 J_v + \beta_3 = 0 \tag{13}$$

where $\beta_1 = 0.5(\sigma_l - \sigma_r)$; $\beta_2 = RT(\omega_l + \omega_r) - 0.5\,L_{pl}L_{pr}(L_{pl} + L_{pr})^{-1}(\sigma_l - \sigma_r)\{(P_l - P_r) + RT[C_l(1 - 2\sigma_l) - C_r(1 - 2\sigma_r)]\}$, $\beta_3 = -L_{pl}L_{pr}(L_{pl} + L_{pr})^{-1}RT\{(P_l - P_r)(\omega_l + \omega_r) - RT(C_l - C_r)(\sigma_r \omega_l + \sigma_l \omega_r)\}$.

Taking into consideration Equations (3), (5), and (7), we obtain

$$J_s = \frac{(\gamma_1 + \gamma_2 J_v{}^2)(C_l - C_r) + \gamma_3 J_v(C_l + C_r)}{\gamma_4 + \gamma_5 J_v} \tag{14}$$

where $\gamma_1 = (RT)^2\omega_l\omega_r$; $\gamma_2 = 0.5(1 - \sigma_l)(1 - \sigma_r)$; $\gamma_3 = 0.5RT[\omega_l(1 - \sigma_r) + \omega_r(1 - \sigma_l)]$; $\gamma_4 = RT(\omega_l + \omega_r)$; and $\gamma_5 = 0.5(\sigma_l - \sigma_r)$.

On the basis of Equations (12)–(14), C_m, J_v, and J_s can be calculated.

J_v and J_s can be used to calculate entropy production (ψ_S) in the double-membrane system, using the expression presented in a previous paper [24]. If there is only an osmotic pressure difference $\Delta\pi = RT\Delta C$ in the double-membrane system, this expression can be written as

$$\psi_S = (\psi_S)_{J_v} + (\psi_S)_{J_s} = RJ_v\Delta C + RJ_s\frac{\Delta C}{\bar{C}} \tag{15}$$

where $(\psi_S)_{J_v}$ is the S-entropy produced by J_v and $(\psi_S)_{J_s}$ is the S-entropy produced by J_s.

3. Results and Discussion

The calculations of $C_m = f(C_l - C_r)$, $J_v = f(C_l - C_r)$, $J_s = f(C_l - C_r)$, $(\psi_S)_{J_v} = f(C_l - C_r)$, and $(\psi_S)_{J_s} = f(C_l - C_r)$ were obtained on the basis of Equations (12)–(15), respectively, for the fixed hydrostatic pressure difference in the double-membrane system $\Delta P = P_l - P_r = 13$ kPa and for two cases: $C_l/M_l/C_m/M_r/C_r$ and $C_l/M_r/C_m/M_l/C_r$. The concentration difference ($\Delta C = C_l - C_h$) has changed in the range from -700 to $+700$ mol m^{-3}. For the M_l and M_r membranes, the following values of transport parameters were used: $\sigma_l = 0.2$, $\sigma_r = 0.1$, $\omega_l = 2 \times 10^{-8}$ mol N^{-1}s^{-1}, $\omega_r = 4 \times 10^{-8}$ mol N^{-1}s^{-1}, $L_{pl} = 2 \times 10^{-9}$ m^{3}N^{-1}s^{-1}, and $L_{pr} = 4 \times 10^{-9}$ m^{3}N^{-1}s^{-1}. The obtained results of these calculations are shown in Figures 2–4, 7 and 8.

In Figure 2, the results of the calculations $C_m = f(C_l - C_r)$ are shown. Parabolas 1 and 1′ were obtained for Case 1, and parabolas 2 and 2′ were obtained for Case 2. Figure 2 shows that parabola 1 crosses the concentration axis at the points $C_l - C_r = -617.6$ mol m^{-3} and $C_l - C_r = 0$, parabola 1′ at the points $C_l - C_r = 0$ and $C_l - C_r = 213.2$ mol m^{-3}. The vertices of these parabolas have the following coordinates: $C_m = 71.7$ mol m^{-3} and $C_l - C_r = -275.7$ mol m^{-3} (parabola 1) and $C_m = 22.8$ mol m^{-3} and $C_l - C_r = 110.3$ mol m^{-3} (parabola 1′). In turn, parabola 2 intersected the concentration axis at the points $C_l - C_r = -165.4$ mol m^{-3} and $C_l - C_r = 0$; parabola 2′ at the points $C_l - C_r = 0$ and $C_l - C_r = 720.6$ mol m^{-3}. The vertices of these parabolas had the following coordinates: $C_m = 13.1$ mol m^{-3} and $C_l - C_r = -84.5$ mol m^{-3} (parabola 2) and $C_m = 90.3$ mol m^{-3} and $C_l - C_r = 305.1$ mol m^{-3} (parabola 2′).

The dotted lines illustrate the dependence of $C_m = f(C_l - C_r)$ for $C_m = 0.5(C_l + C_h)$. The results of the studies presented in Figure 2 indicate that in the double-membrane system, the solution accumulation effect of the intermembrane compartment of this system occurs for parabola 1 if $\sigma_l > \sigma_r$, $\omega_l < \omega_r$, $L_{pl} < L_{pr}$ and -35.9 mol m$^{-3} \geq C_l - C_r < 0$). For parabola 2′, if $\sigma_l < \sigma_r$, $\omega_l > \omega_r$, $L_{pl} > L_{pr}$ and $0 < C_l - C_r \leq 110.3$ mol m^{-3}). For $C_l - C_r < -35.9$ mol m^{-3} (parabola 1) and $C_l - C_r > 110.3$ mol m^{-3} (parabola 2′). For parabola 2 and 1′, the solution depletion effect of the intermembrane compartment of the double-membrane system occurs.
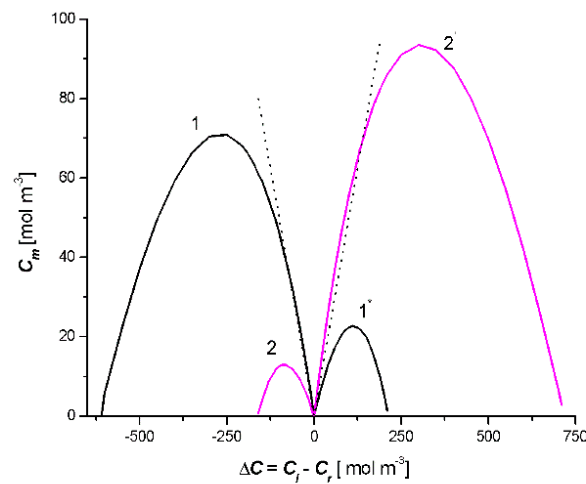
Figure 2. Dependencies $C_m = f(C_l - C_r)$ for the case $C_l/M_l/C_m/M_r/C_r$ (curves 1 and 1′) and $C_l/M_r/C_m/M_l/C_r$ (curves 2 and 2′).

Figure 3 illustrates the results of the calculations of $J_v = f(C_l - C_r)$ based on Equation (13) for Cases 1 and 2. The results of the calculations are shown as the parabola with branches 1a and 1b and the parabola with branches 2a and 2b. The vertex of the first parabola (*C*) had the coordinates: $J_v = -0.92 \times 10^{-3}$ m s^{-1} and $C_l - C_r = 562.1$ mol m^{-3}. The vertex of the second parabola (*B*) had the coordinates: $J_v = 1 \times 10^{-3}$ m s^{-1} and $C_l - C_r = -546.4$ mol m^{-3}. The results of the studies presented in this figure show that the solution of Equation (13) is a pair of parabolas with the common point $J_v = 0$ and $C_l - C_r = 0$.
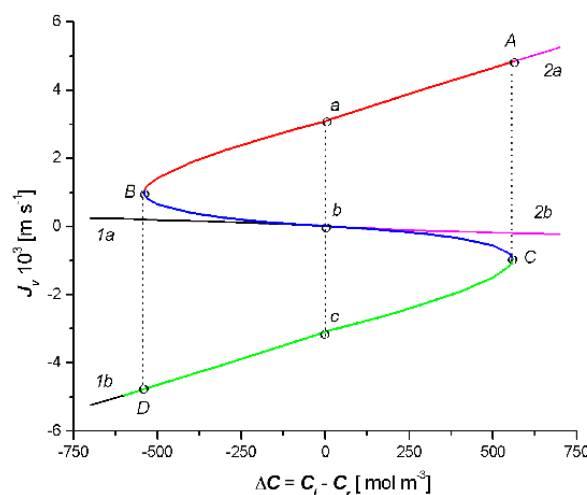

Figure 3. Dependencies $J_v = f(C_l - C_r)$ for the case $C_l/M_l/C_m/M_r/C_r$ (parabola with branches 1a and 1b) and $C_l/M_r/C_m/M_l/C_r$ (parabola with branches 2a and 2b).

Figure 4 presents the results of the calculation of $J_s = f(C_l - C_r)$ based on Equation (14) for the two cases. The obtained results of the calculations are presented as parabolas with branches 1a and 1b and parabola

with branches 2a and 2b. The vertex of the first parabola (*C*) had the coordinates: J_s = 2.4 mol m^{-2}s^{-1} and $C_l - C_r$ = 558.6 mol m^{-3} while the vertex of the second parabola (*B*) $- J_s$ = -2.4 mol m^{-2}s^{-1} and $C_l - C_r$ = -535.1 mol m^{-3}. The results of the studies presented in Figure 4 show that the solution of Equation (14), similar to Equation (13), is a pair of parabolas with a common point, J_s = 0 and $C_l - C_r$ = 0.
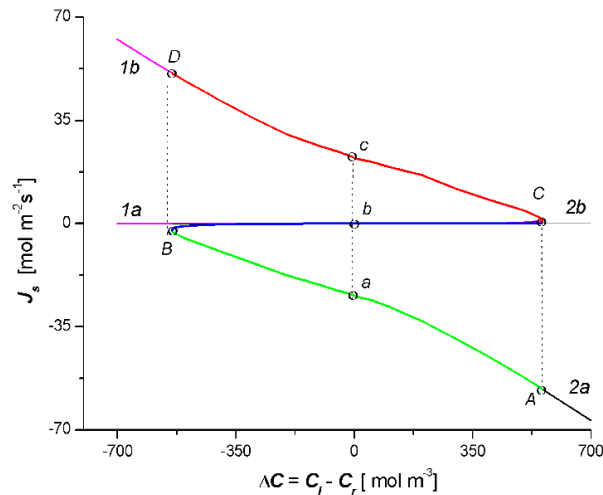

Figure 4. Dependencies $J_s = f(C_h - C_l)$ for the case C_l/M$_l$/C$_m$/M$_r$/C$_r$ (parabola with branches 1a and 1b) and C_l/M$_r$/C$_m$/M$_l$/C$_r$ (parabola with branches 2a and 2b).

We performed the procedure involving the omission of the fragments of the parabolas, which are shown in Figures 3 and 4. If we leave branches 1b and 2a, section Cb of branch 1a of parabola 1 and section Bb of branch 2b, which are shown in Figure 3, we obtain the characteristic $J_v = f(C_l - C_r)$ of the *S* type. Following this procedure for the relation $J_s = f(C_l - C_r)$ (i.e., if we leave branches 1b and 2a, section Cb of branch 2b, and section Bb of branch 1a), which is shown in Figure 4, we obtain the characteristic $J_s = f(C_l - C_r)$ of the reversed letter S type. The curve, which is shown in Figure 3, illustrates the dependence of J_v on the value of the control parameter $\Delta C = C_l - C_r$, when the set value of the parameter $\Delta C_0 = 0$ corresponds to three stationary states of J_{va} = 3.17 × 10^{-3} m s^{-1}, $J_{vb} = 0$, and J_{vc} = 3.0 × 10^{-3} m s^{-1}, respectively. Stable states located on the AB and CD sections of the curve were stable and the states located on the CB section were unstable. When the bifurcating values ΔC_1 = -546.4 mol m^{-3} and ΔC_2 = 562.1 mol m^{-3} were reached, the step transitions CA and BD appeared at the extreme points C and B of the curve, so the unstable states in the BC section never actually occur in real systems [25].

From the curves shown in Figure 3, it follows that for branch 1a in the area $\Delta C = C_l - C_r < 0$, $J_v > 0$ and for branch 2b in the area $\Delta C = C_l - C_r > 0$, $J_v < 0$. Similarly, for segments Bb of curve 2b and Ba of curve 2a, $\Delta C = C_l - C_r < 0$, $J_v > 0$ and for segments Cb of curve 1a and Ca of branch 1b: $\Delta C = C_l - C_r > 0$, $J_v < 0$. This means that, in these ranges of $\Delta C = C_l - C_r$, osmotic transport occurs against the concentration gradient, furthermore, in areas where osmotic transport occurs, despite the concentration gradient $R_v < 0$ (see Figure 7).

In turn, the curve presented in Figure 4 illustrates the dependence of J_s on the value of the control parameter $\Delta C = C_l - C_r$, when the set value of parameter $\Delta C_0 = 0$ corresponds to the three stationary states of J_{sc} = 23 mol m^{-2}s^{-1}, $J_{sb} = 0$, and J_{sa} = -23 mol m^{-2}s^{-1}, respectively. Stationary states located on the AB and CD sections of the curve were stable and the stationary states located on the BC section were unstable. When the bifurcating values of ΔC_1 = -535.1 mol m^{-3} and ΔC_2 = 558.6 mol m^{-3} were reached, the step transitions of CD and BA appeared at the extreme points C and B of the curve, which is shown, so that unstable states on the BC section never actually occur in real systems [26]. In addition, from the curves that are shown in the Figure 4 results, for branch 1b in the area $\Delta C = C_l - C_r < 0$, $J_s > 0$ and for branch 2a in the area $\Delta C = C_l - C_r > 0$, $J_s < 0$. This means that in these ranges of $\Delta C = C_l - C_r$,

the diffusion transport takes place against the concentration gradient and in areas where diffusion transport occurs against the concentration gradient $R_s < 0$ (see Figure 8).

The presented analysis shows that the double-membrane system, which is capable of functioning in one of two stable states, has the properties of a trigger. This means that there is a change from one stable state to another as a result of the change in the value of $\Delta C = C_l - C_r$ and the change in the triad value of the membrane parameters M_l (L_{pl}, σ_l, ω_l) and M_r (L_{pr}, σ_r, ω_r). Trigger properties play an important role in biological systems, defining the directional and stepping transition from one state to another (e.g., in the process of electrical impulse along the nerve fiber transmission or in cell differentiation processes) [25].

Figure 5 presents the results of the calculations $(\psi_S)_{J_v}$ (S-entropy produced by J_v) based on Equation (15). This equation shows that in order to calculate $(\psi_S)_{J_v}$ we need to create the product of the universal gas constant ($R = 8.31$ J mol^{-1}K^{-1}), the results of the calculations J_v (presented in Figure 3) and $\Delta C = C_l - C_r$. Figure 5 shows that $(\psi_S)_{J_v} = f(C_l - C_r)$ is a combination of two curves 1a1b and 2a2b (two crossed bows in the shape of an inverted V), which intersect at the point with the coordinates $(\psi_S)_{J_v} = 0$ and $\Delta C = 0$. It should be noted that the colors of the elements of these curves correspond to the elements of the curves shown in Figure 3: the AB segment in Figure 4 corresponds to the AB segment in Figure 3, the BC segment in Figure 4 corresponds to the BC segment in Figure 3, and the CD segment in Figure 4 corresponds to the CD segment in Figure 3. Simultaneously, the sign $(\psi_S)_{J_v}$ depends on the sign J_v and the sign $\Delta C = C_l - C_r$. The comparison of Figures 3 and 5 shows that for segment AE, the relations $\Delta C > 0$ and $J_v > 0$ were met; for segments *EB* and *BE*, $\Delta C < 0$ and $J_v > 0$; for sections *EC* and *CE*, $\Delta C > 0$ and $J_v < 0$; and for the segment *ED*, $\Delta C < 0$ and $J_v < 0$.
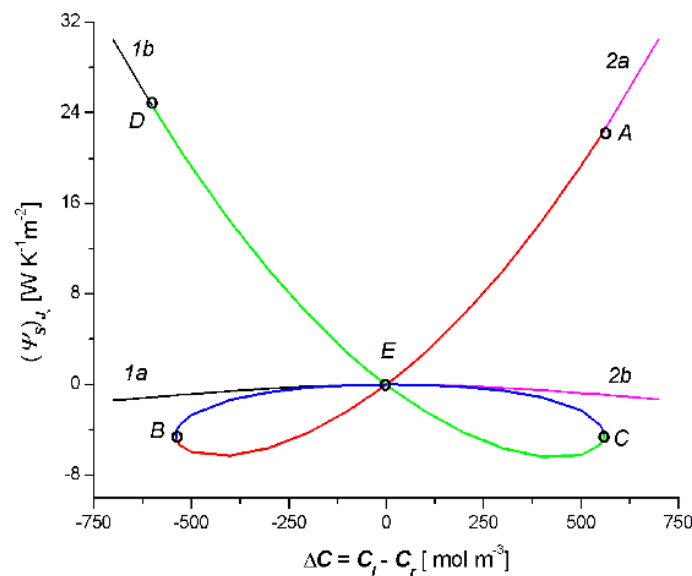

Figure 5. Dependencies $(\Psi_s)_{J_v} = f(C_l - C_r)$ for the case $C_l/M_l/C_m/M_r/C_r$ (curves 1a and 1b) and $C_l/M_r/C_m/M_l/C_r$ (curves 2a and 2b).

Figure 6 shows the results of the calculations $(\psi_S)_{J_s}$ (S-entropy produced by J_s) based on Equation (15). This equation shows that, in order to calculate $(\psi_S)_{J_s}$, we need to create the product of the universal gas constant ($R = 8.31$ J mol^{-1}K^{-1}), the results of the calculations J_s presented in Figure 4, $\Delta C = C_l - C_r$ and $\overline{C}$. Figure 6 shows that $(\psi_S)_{J_s} = f(C_l - C_r)$ is a combination of two curves 1a1b and 2a2b (bow in the shape of a jellyfish), which intersect at the point with the coordinates $(\psi_S)_{J_s} = 0$ and $\Delta C = 0$. It should be noted that the colors of the elements of these curves correspond to the elements of the curves shown in Figure 6: the AC segment in Figure 6 corresponds to the AC segment in Figure 4, the BD segment in Figure 6 corresponds to the BD segment in Figure 4, and the BC segment in Figure 6 corresponds to the BC segment in Figure 4. Simultaneously, the sign $(\psi_S)_{J_s}$ depends on the sign J_s and

the sign $\Delta C = C_l - C_r$. The comparison of Figures 4 and 6 shows that for segment AE, the relations $\Delta C > 0$ and $J_s < 0$ were met; for segments *EC* and *CE*, $\Delta C < 0$ and $J_s < 0$; for segments EB and BE, $\Delta C > 0$ and $J_s > 0$; and for the segment ED, $\Delta C < 0$ and $J_s > 0$.
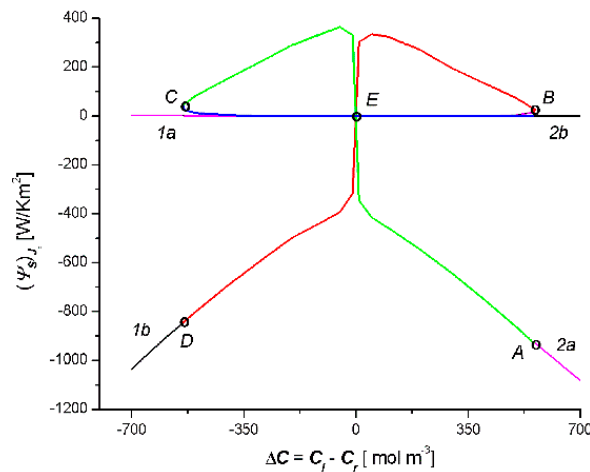

Figure 6. Dependencies $(\Psi_s)_{J_s} = f(C_l - C_r)$ for the case $C_l/M_l/C_m/M_r/C_r$ (curves 1a and 1b) and $C_l/M_r/C_m/M_l/C_r$ (curves 2a and 2b).

Moreover, from Equation (15), it follows that $(\psi_S)_{J_v} > 0$ when simultaneously $J_v > 0$ and $\Delta C > 0$ or when simultaneously $J_v < 0$ and $\Delta C < 0$. In turn $(\psi_S)_{J_s} > 0$, when $J_s > 0$ and $\Delta C > 0$ or $J_s < 0$ and $\Delta C < 0$. When $J_v < 0$ and $\Delta C > 0$ or when $J_v < 0$ and $\Delta C > 0$, then $(\psi_S)_{J_v} < 0$. In the case when $J_s < 0$ and $\Delta C > 0$ or when $J_s < 0$ and $\Delta C > 0$ simultaneously, then $(\psi_S)_{J_s} < 0$. The relations $(\psi_S)_{J_v} < 0$ and $(\psi_S)_{J_s} < 0$ illustrate a deviation from the second law of thermodynamics for the membrane system. From this law, it follows that in the single-membrane system, thermodynamic fluxes reduce the value of stimuli (to which they are induced) and cause an equilibrium state. These thermodynamic fluxes are non-zero until $(\psi_S)_{J_v} > 0$ and $(\psi_S)_{J_s} < 0$. It seems that, in the double-membrane system, due to the occurrence of the phenomenon of accumulation or depletion of the substance in the inter-membrane compartment, cases where $(\psi_S)_{J_v} < 0$ and $(\psi_S)_{J_s} < 0$ are possible.

Applying the results shown in Figures 7 and 8, osmotic resistance (R_v) and diffusion resistance (R_s) were calculated using the following expressions:

$$R_v = \frac{\Delta J_v}{\Delta(C_l - C_r)} \tag{16}$$

$$R_s = \frac{\Delta J_s}{\Delta(C_l - C_r)} \tag{17}$$

The results of these calculations are shown in Figures 7 and 8. It should be noted that curves 1a, 1b, 2a, and 2b (shown in Figure 7) were obtained from curves 1a, 1b, 2a, and 2b (presented in Figure 3). In turn, curves 1a, 1b, 2a, and 2b (shown in Figure 8) were obtained from curves 1a, 1b, 2a, and 2b (presented in Figure 4). Figure 5 shows that $R_v > 0$ for curves 2a and 1b, furthermore, $R_v < 0$ for curves 2b and 1a. Figure 8 shows that $R_s > 0$ for curves 2b and 1a, furthermore, $R_s < 0$ for curves 2a and 1b.

Negative resistance often determines the possibilities of their use of semiconductor components in electronics [26] and membrane systems in physiochemistry [27,28] and biophysics [29]. In membrane systems, negative resistance can be controlled by means of ion currents [29]. Therefore, the mechanism of negative resistance is the basis for the excitation of bio membranes [30].

All data were entered and calculated in Microsoft Excel 2016 and Origin Pro 2020.
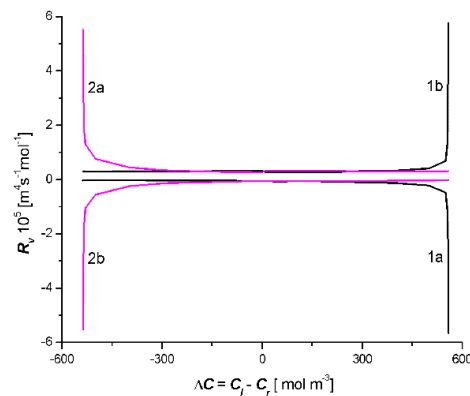
Figure 7. Dependencies $R_v = f(C_l - C_r)$ for the case $C_l/M_l/C_m/M_r/C_r$ (curves 1a and 1b) and $C_l/M_r/C_m/M_l/C_r$ (curves 2a and 2b).
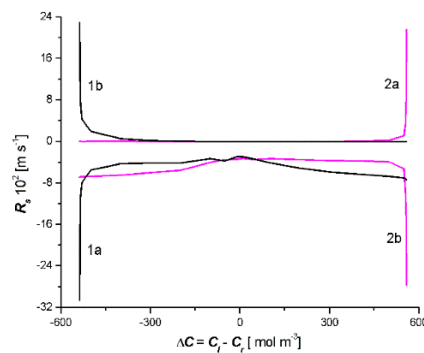

Figure 8. Dependencies $R_s = f(C_h - C_l)$ for the case $C_l/M_l/C_m/M_r/C_r$ (curves 1a and 1b) and $C_l/M_r/C_m/M_l/C_r$ (curves 2a and 2b).

4. Conclusions

These investigations showed that:

1. We created nonlinear model equations of the concentration in the inter-membrane compartment (C_m), volume flux (J_v), solute flux (J_s), and S-entropy produced by J_v, $\left((\psi_S)_{J_v}\right)$ and by J_s $\left((\psi_S)_{J_s}\right)$ for binary homogeneous, non-electrolyte solutions. The created model equations, illustrated by Equations (12)–(15), consist of quadratic equations describing the concentration in the inter-membrane compartment (C_m), volume flux (J_v), and solute flux (J_s) through the double-membrane system.

2. The double-membrane system, composed of two membranes (M_l, M_r), separates the compartments *l*, *m*, and *r* containing the homogeneous, non-electrolyte binary solutions. The compartment *m* consists of the infinitesimal layer of the solution and its volume fulfills the condition $V_m \to 0$. The volume of the compartments *l* and *r* fulfills the condition $V_l = V_r \to \infty$. At the initial moment, the solution concentrations in the cell satisfy the condition $C_l < C_m < C_r$.

3. Based on this model, for the fixed values of the reflection (σ_l, σ_r), hydraulic permeability (L_{pl}, L_{pr}), and solute permeability (ω_l, ω_r) coefficients, the dependencies $C_m = f(C_l - C_r)$, $J_v = f(C_l - C_r)$ and $J_s = f(C_l - C_r)$ were calculated. Each of the obtained characteristics was specifically arranged as a pair of parabolas.

4. The relationship $(\psi_S)_{J_v} = f(C_l - C_r)$ was a combination of two curves, 1a1b and 2a2b (two crossed bows in the shape of an inverted V), which intersected at the point with the coordinates $(\psi_S)_{J_v} = 0$ and $\Delta C = 0$. The sign $(\psi_S)_{J_v}$ was the consequence of the sign J_v and ΔC: $(\psi_S)_{J_v} > 0$ when simultaneously $J_v > 0$ and $\Delta C > 0$, or when simultaneously $J_v < 0$ and $\Delta C < 0$. If simultaneously $J_v < 0$ and $\Delta C > 0$ or when simultaneously $J_v < 0$ and $\Delta C > 0$, then $(\psi_S)_{J_v} < 0$. In turn, the relationship

$(\psi_S)_{J_s} = f(C_l - C_r)$ is a bow in the shape of a jellyfish. The sign $(\psi_S)_{J_s}$ was the consequence of the sign J_s and ΔC: $(\psi_S)_{J_s} > 0$ when simultaneously $J_s > 0$ and $\Delta C > 0$ or when simultaneously $J_s < 0$ and $\Delta C < 0$. If simultaneously $J_s < 0$ and $\Delta C > 0$ or when simultaneously $J_s < 0$ and $\Delta C > 0$, then $(\psi_S)_{J_s} < 0$. The cases $(\psi_S)_{J_v} < 0$ and $(\psi_S)_{J_s} < 0$ indicate a deviation from the second law of thermodynamics caused by the phenomenon of the accumulation or depletion of the dissolved substance in the inter-membrane compartment of the double-membrane system.

5. In the solution concentration areas, where the relations were $\Delta C < 0$, $J_v > 0$ and $J_s > 0$, $\Delta C > 0$, $J_v < 0$ and $J_s < 0$, osmotic and diffusion transport (against the concentration gradient) occurred. In addition, in the areas where osmotic and diffusive transport took place (against the concentration gradient), osmotic and diffusion resistances (R_v, R_s) satisfied the conditions $R_v < 0$ and $R_s < 0$.

References

1. Demirel, Y. *Nonequilibrium Thermodynamics: Transport and Rate Processes in Physical, Chemical and Biological Systems*; Elsevier: Amsterdam, The Netherlands, 2014; pp. 275–540, ISBN 978-0-444-53079-0.
2. Srivastava, R.C.; Saha, S.K.; Jain, A.K. *Thermodynamics: A Core Course*; PHI Learning: New Delhi, India, 2010; pp. 214–273, ISBN 978-81-203-3296-6.
3. Delmotte, M.; Chanu, J. Non-equilibrium thermodynamics and membrane potential measurement in biology. In *Topics Bioelectrochemistry and Bioenergetics*; Millazzo, G., Ed.; John Wiley Publish & Sons: Chichester, UK, 1979; pp. 307–359.
4. Prigogine, I. *Introduction to Thermodynamics of Irreversible Processes*; Wiley: New York, NY, USA, 1968.
5. Baker, R. *Membrane Technology and Application*; John Wiley & Sons: New York, NY, USA, 2012; ISBN 978-0-470-74372-0.
6. Cheng, X.; Pinsky, P.M. The balance of fluid and osmotic pressures across active biological membranes with application to the corneal endothelium. *PLoS ONE* **2015**, *10*, e0145422. [CrossRef] [PubMed]
7. Jadhav, S.V.; Marathe, K.V.; Rathod, V.K. A pilot scale concurrent removal of fluoride, arsenic, sulfate and nitrate by using nanofiltration: Competing ion interaction and modelling approach. *J. Water. Proc. Eng.* **2016**, *13*, 153–167. [CrossRef]
8. Teugels, L. Double Membrane Transducer Protector. U.S. Patent No 7,516,665 B2, 14 April 2009.
9. Yan, Y.; Gu, S.; Gong, K. Double-Membrane Triple-Electrolyte Redox Flow Battery Design. U.S. Patent No. 9,917,323 B2, 13 March 2018.
10. Curran, P.F.; McIntosh, J.R. A model system for biological water transport. *Nature* **1962**, *193*, 347–348. [CrossRef] [PubMed]
11. Patlak, C.S.; Goldstein, D.; Hoffman, J.F. The flow of solute and solvent across a two-membrane system. *J. Theor. Biol.* **1963**, *5*, 426–442. [CrossRef]
12. Richardson, I.W. Multiple membrane system as biological models (current-voltage behavior). *J. Membr. Biol.* **1972**, *8*, 219–236. [CrossRef] [PubMed]
13. Ginsburg, H. Model for iso-osmotic water flow in plant roots. *J. Theor. Biol.* **1971**, *32*, 147–158. [CrossRef]
14. Kedem, O.; Katchalsky, A. Permeability of composite membranes. Part 3. Series array of elements. *Trans. Faraday Soc.* **1963**, *59*, 1941–1953. [CrossRef]
15. Katchalsky, A.; Curran, P.F. *Nonequilibrium Thermodynamics in Biophysics*; Harvard University Press: Cambridge, MA, USA, 1965; ISBN 9780674494121.
16. Naparstek, A.; Caplan, S.R.; Katzir-Katchalsky, A. Series arrays of ion-exchange membranes concentration of electric current. *Israel J. Chem.* **1973**, *11*, 255–270. [CrossRef]
17. Ohki, S. Rectification by double membranes. *J. Phys. Sci. Jpn.* **1965**, *20*, 1674–1685. [CrossRef]

18.　Tsukahara, S.; Nanzai, B.; Igawa, M. Selective transport of amino acids across a double membrane system composed of a cation- and an anion-exchange membrane. *J. Membr. Sci.* **2013**, *448*, 300–307. [CrossRef]

19.　Ueno, K.; Doi, T.; Nanzai, B.; Igawa, M. Selective transport of neutral amino acids across a double-membrane system comprising cation and anion exchange membranes. *J. Membr. Sci.* **2017**, *537*, 344–352. [CrossRef]

20.　Kargol, M.; Dworecki, K.; Przestalski, S. Graviosmotic flow amplification effects in a series membrane system. *Stud. Biophys.* **1979**, *76*, 137–144.

21.　Ślęzak, A.; Wasik, J.; Ślęzak, K. Effect of concentration boundary layers on mechanical pressure in a double-membrane system. *Desalination* **2004**, *168*, 423–433. [CrossRef]

22.　Ślęzak, A.; Wasik, J.; Grzegorczyn, S. Irreversible thermodynamics model equations for heterogeneous solute flux in a double-membrane system. *Desalination* **2004**, *163*, 155–175. [CrossRef]

23.　Ślęzak, A.; Jasik-Ślęzak, J.; Grzegorczyn, S.; Ślęzak-Prochazka, I. Nonlinear effects in osmotic volume flows of electrolyte solutions through double-membrane system. *Transp. Porous Med.* **2012**, *92*, 337–356. [CrossRef]

24.　Ślęzak, A.; Ślęzak-Prochazka, I.; Grzegorczyn, S.; Jasik-Ślęzak, J. Evaluation of S-Entropy production in a single-membrane system in concentration polarization conditions. *Trans. Porous Med.* **2017**, *116*, 941–957. [CrossRef]

25.　Rubin, A.B. *Thermodynamics of Biological Processes*; Moscow State University Press: Moscow, Russia, 1984.

26.　Weber, W.H.; Ford, G.W. Double injection in semiconductors heavily doped with deep two-level traps. *Solid-State Electron.* **1970**, *13*, 1333–1356. [CrossRef]

27.　Anderson, J.E. A model for current-controlled negative resistance in ion/membrane systems. *J. Membr. Sci.* **1978**, *4*, 35–40. [CrossRef]

28.　Abu-Rjal, R.; Prigozhin, L.; Rubinstein, I.; Zaltzman, B. Teorell instability in concentration polarization. *Phys. Rev. E* **2015**, *92*, 022305. [CrossRef] [PubMed]

29.　Franck, U.F. Phänomene an biologischen und künstlichen membrane. *Berichte Bunsengess.* **1967**, *71*, 789–799. [CrossRef]

30.　Cole, K.S. *Membranes, Ions and Impulses*; University California Press: Berkeley, CA, USA, 1968; ISBN 0-520-00252-2.